doi:10.22364/mmp2017.28

VIII International Scientific Colloquium
Modelling for Materials Processing
Riga, September 21 - 22, 2017

Self-Adaptive Multimethod Optimization Search Applied to a Tailored Heating Forging Process

M. Baldan, T. Steinberg, E. Baake

Abstract

The presented paper shows the use of a self-adaptive multi-objective optimization code applied to a "tailored" heating forging process. The choice of the frequency and the time are followed by the inductor's design. Finally, a straightforward optimization is performed in order to show how "optimal control" can be applied.

Introduction

Evolutionary algorithms have been successfully applied in the last few decades for solving optimization and design problems of electromagnetic devices [1]. The goal is to determine values for model parameters that provide the best trade-off in the case of multiple conflicting objects. We consider a multi-objective optimization problem, with n decision variables: $\boldsymbol{x} = (x_1,\ldots x_n)$ and m objectives: $f(\boldsymbol{x}) = (f_1(\boldsymbol{x}),\ldots, f_m(\boldsymbol{x}))$ subject to $g_i(\boldsymbol{x}) \leq 0\ i = 1,2,\ldots,r$ and $h_i(\boldsymbol{x})=0\ i =1,2,\ldots s$. The presence of multiple objectives give rise to a set of Pareto-optimal solutions, instead of a single solution. A Pareto-optimal solution is one in which one objective cannot be further improved without causing a simultaneous degradation in at least one other objective.

Currently, the non-dominated sorted genetic algorithm (NGSA-II) [2] has received the most attention because of its simplicity and demonstrated superiority over other methods and it has been widely used in the design of electromagnetic devices [3]. Particle Swarm Optimization (PSO) [4] is a heuristic search technique that simulates the movement of a flock of birds which aim to find food. The relative simplicity of PSO and the fact that it is a population based technique have made it a natural candidate to be used in design problems [5]. On the other hand, in computational electromagnetics, applications and also modifications of Biogeography-Based Optimization (BBO) are an emerging new field of research [6]. However, it has been proved that it is impossible to develop a single algorithm that is always efficient for a diverse set of optimization problems [7].

Inspired by the work of Vrugt et al. [8], we present an optimization procedure which combines the concepts of simultaneous multimethod search and self-adaptive offspring creation. We intend to apply this innovative optimum search not only to few benchmark problems but also to a real inductor's design case addressed to tailored heating applications.

1. Proposed optimization method

The algorithm here used is a modification of the algorithm AMALGAM proposed by Vrugt et al. [8]. We'll call it, for the sake of simplicity, AMALGAM*. In Figure 1 is shown the main procedure of the optimization code. The algorithm is initialized by using a random population P_0 of size N. Then, to each parent is assigned a fitness value based on the non-

dominated sorting mode [2]. The population of offspring $Q_0 = \{Q_0^1, \dots, Q_0^k\}$, is implemented using *k* individual algorithms instead of using a single operator. The chance that one offspring is generated by the *k-th* algorithm is proportional to the "specific probability" *k-th* of the algorithm itself. If at the beginning each algorithm has the same "specific probability", at each generation, the values are updated according to the success that algorithms have in producing offspring. The idea of using the "specific probability" is an original contribution of the authors. After offspring's creation, a combined population $R_0 = P_0 \cup Q_0$ of size *2N* is created and ranked using the non-dominated sorting mode. The N members for the next population are chosen according to the rank and the crowding distance of the *2N* elements of R_0. The new population P_1 is then used to create offspring using the already described procedure. This step algorithm is repeated until convergence is reached.

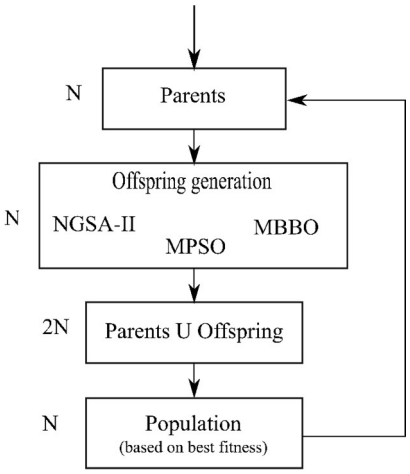

Fig. 1. Flowchart of the proposed algorithm

If the vector $\{S_t^1, \dots, S_t^k\}$ indicates the "specific probability" at *t* generation, $\{N_{t-1}^1, \dots, N_{t-1}^k\}$ is the number of offspring that, at the previous generation, each algorithm generated and, $\{P_t^1, \dots, P_t^k\}$ stands for the number of offspring, produced by the *k-th* algorithm, which appear in the current population, the "specific probability" has been calculated as follows(1):

$$S_t^i = \frac{P_t^i / N_{t-1}^i}{\sum_{j=1}^{k} P_t^j / N_{t-1}^j} \quad (1)$$

In order to avoid inactivating algorithms, the minimum "specific probability" value was set to 0.1. In AMALGAM*, we adopted three different algorithms for generation offspring: Non dominated sorting genetic algorithm NGSA-II [2], Multi-objective particle swarm optimization MPSO [4], Multi-objective biogeography-based optimization MBBO [6,9].

NGSA-II uses simulated binary crossover (SBX) and polynomial mutation to create offspring. In the case of MPSO, let $\vec{x}_h(t)$ denote the position of the *h-th* particle at the iteration t, the position of the particle is changed by adding a velocity $\vec{v}_h(t)$ to the current position:

$$\vec{x}_h(t) = \vec{x}_h(t-1) + \vec{v}_h(t) \quad (2)$$

The velocity vector reflects the socially exchanged information. In the case of MPSO, since there is not – like in the single objective case – a best solution, the "best" particle is a random one extracted from an external archive which contains the best $\|\exp(e^{2m})\|$ non-dominated particles (particles are sorted by rank and crowding distance). The best particle's position ever is instead updated when the particle is dominated of if both are incomparable (they are both non-dominated with respect to each other).

In MBBO each solution considered is treated as habitat. The offspring are generated by means of two stochastic operators: migration and mutation. Migration is supposed to improve "bad" habitats (which have bad fitness) by sharing features from "good" habitats. Mutation modifies some randomly selected habitats in view of a better exploration of the design space.

In case of constrained optimization, if an offspring (particle) violates one or more constraints in the design space, objective functions are not evaluated. What it is calculated is the "violation", i.e. $v_h = \sum_{q=1}^{r} \max\left(0, g_q(\boldsymbol{x})\right) + \sum_{q=1}^{s} \left|h_q(\boldsymbol{x})\right|$. Each feasible solution has a better fitness than every other unfeasible solution. Unfeasible solutions are ranked on the basis of their v_h: the smaller v_h, the better the fitness.

2. Numerical test

In this section we intend to test AMALGAM* applying it to four analytical cases. We adopt the metrics used in [10] to quantify the performance of the proposed algorithm. We

evaluate the error between the approximated and exact one, both in the Pareto front (objective function space) and its correspondent inverse image (variable space). Considering N_{fr} individuals with the lowest rank final front, the geometric distance between each *h-th* point $\boldsymbol{x} = (x_1, \ldots x_n)$ and its inverse image is:

$$d_{x,h} = \sqrt{\sum_{i=2}^{n} \left(x_{i,h} - \boldsymbol{f_i^{-1}}(x_{1,h}, \ldots x_{n,h})\right)^2} \qquad (3)$$

Where $\boldsymbol{f_i^{-1}}$ is the *i-th* component of the inverse image of the Pareto front.
While, in order to evaluate the error in the objective space, in the case of two objective functions:

$$d_{f,h} = \left|f_{2,k} - \boldsymbol{f_{2,k}}(f_{1,k})\right| \qquad (4)$$

With $\boldsymbol{f_{2,k}}$ is given the exact expression of the Pareto front. The rms error value of the N_{fr} distances is evaluated in order to compare the performances.
The so called "relative" crowding distance has been also calculated for both the objective and variable spaces. The average "relative" distance of N_{fr} individuals in the variable space is:

$$\sigma_x = \frac{1}{N_{fr}-1}\sqrt{\sum_{i=1}^{n}\left[\frac{\max(x_i)-\min(x_i)}{\max(x_i)-\min(x_i)}\right]^2} = \frac{\sqrt{n}}{N_{fr}-1} \qquad (5)$$

An analogous expression is used in the objective space, where *n* is substituted with *m* (the space's dimension). The average relative distance is called here σ_f.
In the variables space, the relative distance between the *h-th* and the j-*th* individuals, both in the front, is:

$$d_x(h,j) = \sqrt{\sum_{i=1}^{n}\left[\frac{x_{h,i}-x_{j,i}}{\max(x_i)-\min(x_i)}\right]^2} \qquad h \neq j \qquad (6)$$

Again, for the objective space, it's just sufficient to substitute *n* with *m* and *x* with *f*.
The crowding of the front in terms of design variables $cw_x(h)$ is the number of individuals, *j-th*, which are closer to the individual *h-th* than the threshold σ_x:

$$cw_x(h) = \sum_{j=1}^{N_{fr}} U_{h,j} \quad \text{with } U_{h,j} = \begin{cases} 1 & if\ d_x(h,j) < \sigma_x \\ 0 & if\ d_x(h,j) \geq \sigma_x \end{cases}$$

Also here there is a correspondent definition for the objective space.

2.1 Test functions

We considered four unconstrained test functions [2,10,11] which are summarized in Table 1:

Tab. 1. Test functions: T1, F2, ZDT1, ZDT4.

	n	Variable bounds	Objective functions	Optimal solutions	Pareto front
A	2	[0,2]	$f_1 = x_1^2 + x_2^2$ $f_2 = (x_1-1)^2 + (x_2-1)^2$	$x_1 = x_2$	$f_2 = f_1 - 2\sqrt{2f_1} + 2$
B	3	$x_1 \in [0,1]$ $x_2, x_3 \in [-1,1]$	$f_1 = x_1 + \frac{2}{3}[x_3 - \sin(6\pi x_1 + \pi)]^2$ $f_2 = 1 - \sqrt{x_1} + \left[x_2 - \sin\left(6\pi x_1 + \frac{2}{3}\pi\right)\right]^2$	$x_i = \sin\left(6\pi x_1 + \frac{i\pi}{n}\right)$ $i = 2,..,n$	$f_2 = 1 - \sqrt{f_1}$
C	30	[0,1]	$f_1 = x_1$ $f_2 = g(x)[1 - \sqrt{x_1/g(x)}]$ $g(x) = 1 + 9(\sum_{i=2}^{n} x_i)/(n-1)$	$x_i = 0$ $i = 2,..,n$	$f_2 = 1 - \sqrt{f_1}$
	10	$x_1 \in [0,1]$ $x_i \in [-5,5]$, $i \neq 1$	$f_1 = x_1$ $f_2 = g(x)[1 - \sqrt{x_1/g(x)}]$ $g(x) = 1 + 10(n-1)$ $+ \sum_{i=2}^{n}[x_i^2 - 10\cos(4\pi x_i)]$	$x_i = 0$ $i = 2,..,n$	$f_2 = 1 - \sqrt{f_1}$

Table 2. Comparison of rms error in the variable and objective space

Test	Pop	Gen	Code	$err_{rms}(x)$	$err_{rms}(f)$
A	20	20	NGSA-II	0.205	0.068
			AMALGAM*	0.0819	0.0202
A	20	50	NGSA-II	0.125	0.0333
			AMALGAM*	0.0497	0.0118
B	20	50	NGSA-II	0.478	0.332
			AMALGAM*	0.186	0.0511
B	20	100	NGSA-II	0.408	0.3086
			AMALGAM*	0.1377	0.0285
C	100	200	NGSA-II	0.914	0.698
			AMALGAM*	0.0633	0.0398
D	100	300	NGSA-II	**	**
			AMALGAM*	0.4982	0.1838

Tests were performed with 20 different starting populations. Here we present the average (over the 20 cases) rms error in both variable and objective spaces, as the most representative indicator in the ability to identify the Pareto front.

With "*Pop*" and "*Gen*" we refer respectively to population's individuals number (called it *N* before) and to the generations' number. In other words, we decide a priori the number of calls of the objective functions.

In every case AMALGAM* shows an evident superiority compared to NGSA-II. In the case D (**), at every attempt, the code NGSA-II failed the convergence to the real Pareto front. We show here more in details the results in case of test A.

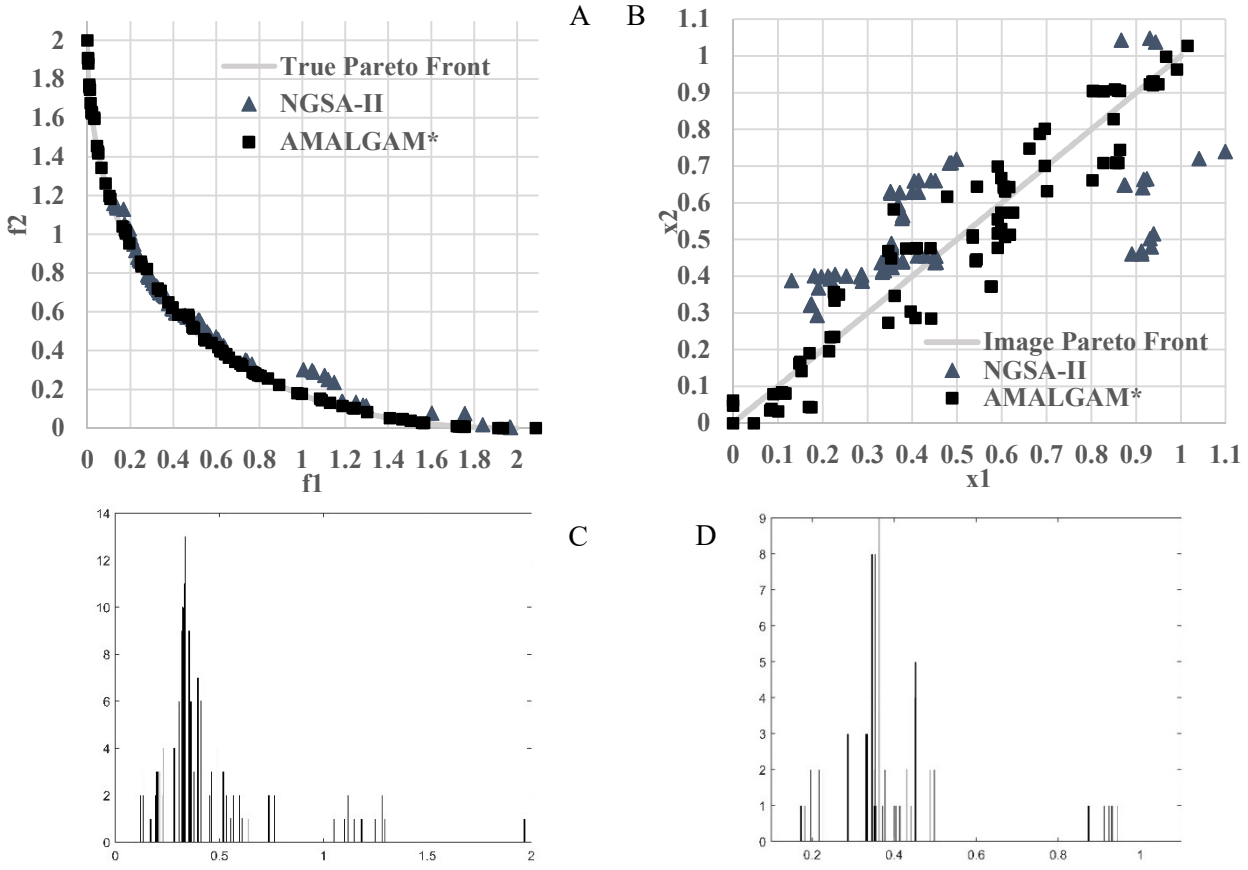

Figure 2. Comparison between calculated and true Pareto front in the objective (A) and variable (B) spaces with *Pop*=20 and *Gen*=20. Crowing distances in ***f*** space with NGSA-II (C) and AMALGAM* (D)

A better ability of exploiting the Pareto front is shown by AMALGAM* compared to NGSA-II. Especially in the left side, results obtained with NGSA-II don't cover the overall extension of the Pareto front. This fact is visible in the calculation of the crowding distance: particles amass much more in the case of NGSA-II (see Figure 2).

3. Tailored heating

In literature the concept of "Tailored heating" refers to an innovative heating approach which is addressed to forging processes [12]. Forging a billet from an initially "simple" geometry to a part of "complex" geometry may require several preform stages. In each stage, a pair of dies must be designed and manufactured. Subsequently, a series of mounting and dismounting die-inserts must be performed in the preform stage. This is often time consuming and costly. Consequently, the die forging of parts with complex geometry is only cost effective for large-batch production. Guo et al. [13] and Kayatürk et al. [14] proposed a thermal differential flat-die forging process, in which the parts of the forging billets which are supposed to have a high material flow are heated up to hot forging temperature. Parts which are supposed not to have such high material flow are at "colder" temperatures like 800-900 [°C]. This contains the basic idea of "Tailored heating".

The work-piece under analysis is a 42CrMo4 carbon steel billet with 474 [mm] length and 30 [mm] diameter. The problem aims to heat up the billet with a desired temperature profile: two "hot" zones with a uniform temperature of 1200 [°C] alternate with three "cold" zones which are supposed to reach a uniform temperature of 900 [°C]. It was considered a coupled electromagnetic-thermal model for the field analysis with the package ANSYS®.
The design of an inductor which is able to provide the afore described temperature profile is the topic of this work. It represents a challenging task in which AMALGAM* has been applied.

3.1 Choice of frequency and heating time

We want to understand which frequency- heating time couple best fits to our purpose. In [12] good results have been reached using a frequency of 4 kHz and a heating time of 70 seconds. We consider for simplicity a 1D model (Figure 3), in which the inductor is a massive piece of copper and the billet is substituted with a work-piece whose thickness is equal to the billet's radius.

Our intention is to obtain a uniform temperature of 1200 [°C]. Two objective functions are evaluated: the maximum deviation, at the end of the heating, along the line A-B (see Figure 3) from 1200 [°C] and the energy consumption (7). A fixed current is applied for the entire duration of the heating.

$$f_1 = \max|T(l_{AB}, t_{heat}) - 1200°| \qquad f_2 = \int_{t_{heat}} E\, dt \qquad (7)$$

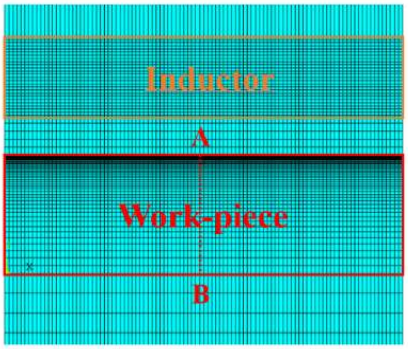

Fig. 3. Geometry of the model

Three design parameters are under investigation: heating time (t), frequency (f) and current (I) (Table 3). Values of current don't have a real physical meaning because we are referring to a 1D model.

Figure 4 summarizes the results of optimization after 100 generations with a population of 20 individuals. While AMALGAM* shows a greater ability in exploring the Pareto front compared to the results obtained with NGSA-II, the minimum value of *f1* is practically the same (see Table 4).

Tab. 3. Parameters to be optimized

t	f	I
40-70 [s]	4-7 [kHz]	4-7 [kA]

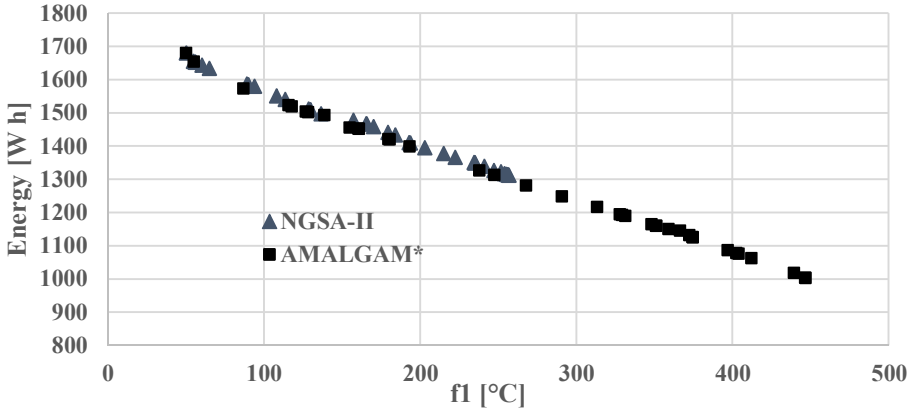

Fig. 4. Approximated Pareto front

Tab. 4. Point with the minimum value of f1 (heating accuracy)

Minimum f_1					
	t [s]	**f [kHz]**	**I [A]**	**f_1 [°C]**	**f_2 [Wh]**
NGSA-II	69.8	4	4634	50.9	1682
AMALGAM*	70	4	4626	50.0	1681

As expectable, the maximum homogenization is obtained with longest time and the smallest frequency. What is interesting to see, is that, moving along the Pareto front, with a frequency of 4 [kHz] and a heating time of 63 [s], f1 values 55°C, which is only 5°C more than the found optimum with minimum f1. On the other hand, the energy consumption is in this case 1655 [Wh] (1.6% less) and the time is drastically reduced. For this reason, we adopt a frequency of 4 [kHz] and a heating time of 63 [s]. In Figure 5 instead are shown the trends of the "specific probability" during the 100 generations of the three optimization algorithms used in AMALGAM*. If at first NGSA-II and MBBO are dominant, the Particle Swarm shows a better ability in exploiting the Pareto front. That's why it has the maximum specific probability in the last generations.

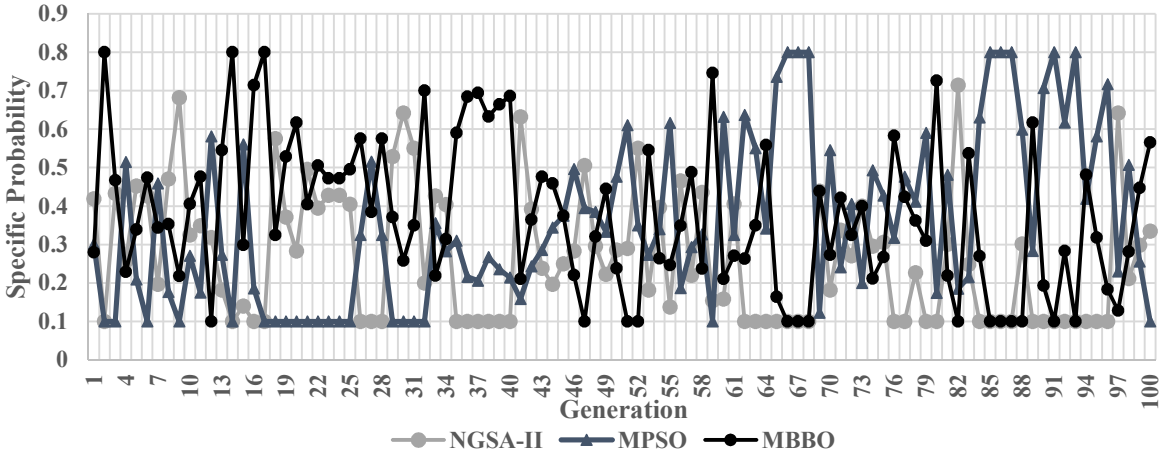

Fig. 5. Specific probability of NGSA-II, MPSO and MBBO during the 100 generations

3.2 Inductor's design

The next step is the design of the inductor. Since it's very difficult to define a priori the inductor's configuration (number of turns, air gaps between them…), in the model proposed the inductor is substituted by five nonconductive areas in each of them a uniform current density is applied. In order to speed up the solution, the numerical model consists of one fourth of the

system (Figure 6). As design variables, the length l_i and the current density j_i applied to each area are considered. l_0 indicates the position of the first area from the middle of the billet. In total 11 variables are under analysis:

Tab. 5. Design variables in the inductor's design problem

l_0	l_1 [mm]	l_2	l_3	l_4	l_5
1-10	20-60	5-20	70-150	5-40	40-150
	j_1 [A/m^2]	j_2	j_3	j_4	j_5
	0.5-1 10^7	0.1-0.8 10^7	0.8-1.35 10^7	0.1-0.9 10^7	0.6-1.3 10^7

The aim is to obtain a uniform temperature of 1200 [°C] in the hot zone and 900 [°C] in the cold ones. As visible in Figure 6, we don't take into account the temperature between different zones, in a transition zone 15 [mm] long.

Three objective functions are evaluated:

$$\begin{aligned} f_1 &= \sum_{i=1}^{W} |T(x_i, y_i, t_{heat}) - 900°| \\ f_2 &= \sum_{i=1}^{Q} |T(x_i, y_i, t_{heat}) - 1200°| \\ f_3 &= \sum_{i=1}^{Z} |T(x_i, y_i, t_{heat}) - 900°| \end{aligned} \quad (8)$$

Each objective function is the sum of the differences between the desired and calculated temperature in a particular zone at the end of the heating. The huge number of variables require a great amount of goal functions' evaluations. A population of 40 individuals after 70 generations has given these results in terms of goal functions (Fig. 7):

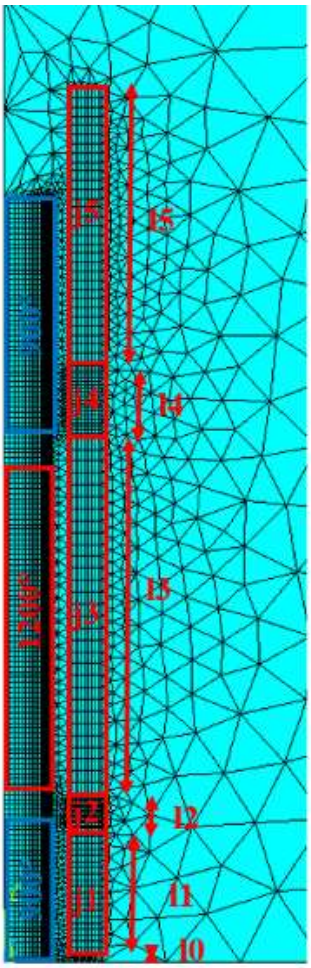

Fig. 6. Geometry of the model

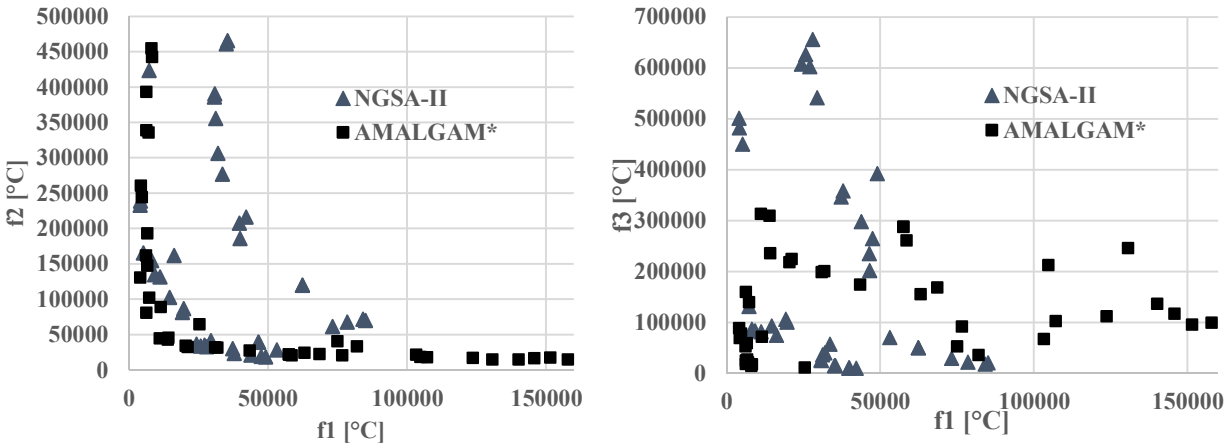

Fig. 7. Results of optimization after 2800 goal functions evaluations

For the design of the inductor we consider the closest solution to the "utopia" point (Table 6).

Tab. 6. Best solution for the inductor's design.

	l_0	l_1	l_2	l_3	l_4	l_5	f_1	f_2	f_3
[mm]	2.4	20.1	12.9	114.0	18.4	109.5	25.45 10^3 [°C]	65.17 10^3 [°C]	11.45 10^3 [°C]
		j_1	j_2	j_3	j_4	j_5			
[A/m^2]		0.999 10^7	0.129 10^7	1.118 10^7	0.433 10^7	0.798 10^7			

3.3 Real inductor

As already done in [12], we need to "translate" this configuration in a real inductor. Each area could be seen as one turn coil. For designing the real inductor, assuming a series connection between turns, it's possible to convert every one-turn coil in an equivalent multi-turns coil using the Ampere's law. The total equivalent current (current density times area) which flows in each area is visible in Table 7.

Tab. 7. Total equivalent current

I1	I2	I3	I4	I5
2008 [A]	166 [A]	12745 [A]	797 [A]	8738 [A]

The number of turns in each zone has been chosen as follows: 2 in the first, 7 in the second and 6 in third. In total there are 15 turns in a half inductor, which are equally distributed in each area. The resulting temperature profile is bell-shaped at the centre of the "hot" zone due to the fact that there the magnetic field is maximum. For this reason, a new sub-optimization is performed, in which, the positions of the turns are modified in order to get a more satisfying temperature profile. In this case 13 variables are under analysis: the y positions of the first 12 turns plus the (assumed) constant distance of the last three turns (see Figure 8).
Since the overlapping between turns is not allowed, we're looking at a constrained optimization case. We set a minimum distance between turn and turn of 1 [mm]. Using a coil with an external diameter of 10 [mm], the following inequalities must be true:

$$y_{i+1} - y_i \geq 11 \text{ mm with } i = 1,...,11 \qquad (9)$$

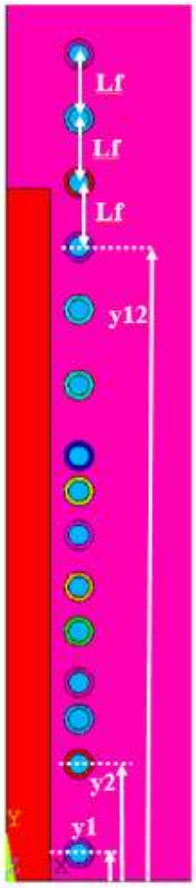

Fig. 8. Geometry of the real inductor's optimization

In Table 8 the variables' domains and the solution which best meets our purposes are summarized. Goal functions are the same that have already been used (8). A population of 30 individuals had been run for 100 generations. The total number of evaluations is 2384 for the NGSA-II and 2375 in the case of AMALGAM*.

Tab. 8. Design parameters and best solution obtained.

	y_1	y_2	y_3	y_4	y_5	y_6	y_7	y_8	y_9	y_{10}	y_{11}	y_{12}	L_f
Min [mm]	8.5	38	50	64	80	95	110	127	142	165	190	210	18
Max [mm]	12	43	60	74	90	105	125	140	155	180	201	225	26
Best [mm]	9.5	40	55.4	68	85.5	100.7	118.5	133.5	144.5	169.8	195.7	217.1	22.0

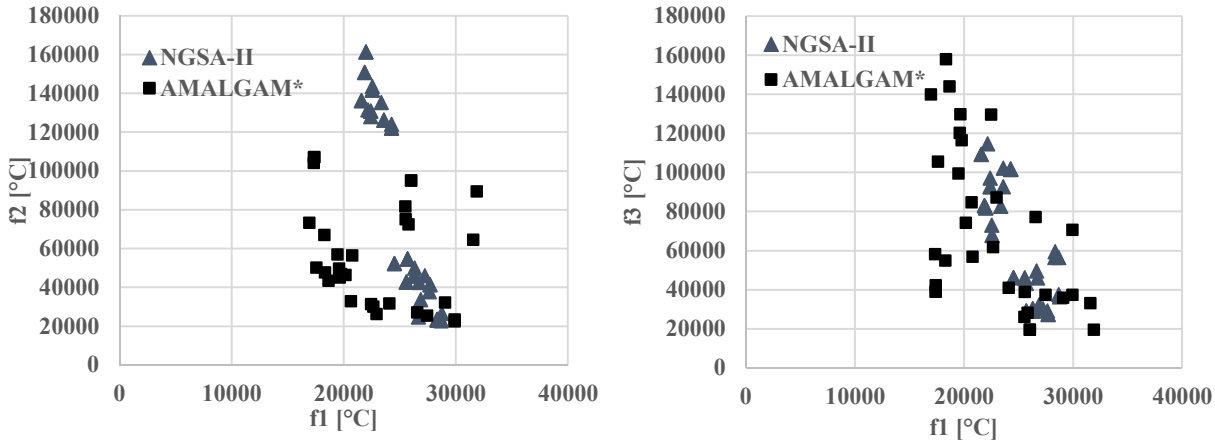

Fig. 9. Results of optimization in the real inductor case

Figure 10 shows the temperature distribution along the length evaluated in the centre and in the surface in the case of what we consider the best "solution". We preferred a solution in which f_2 is pretty low rather than f_1 and f_3.

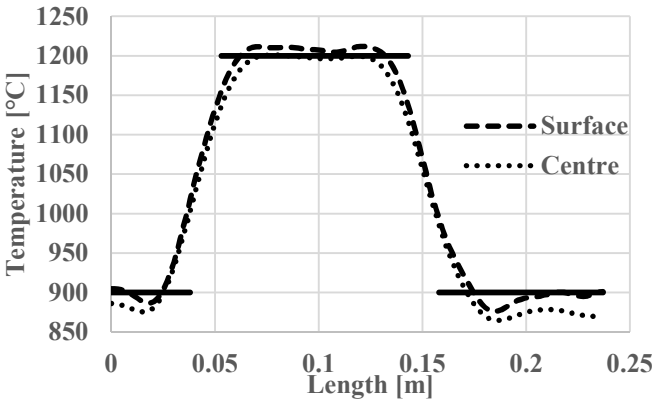

Fig. 10. Temperature profile along the length at the surface and in the centre

3.4 Optimal control

In this last section we intend to apply the concept of optimal control to the already designed inductor. Typically, optimal control applications are performed with a defined voltage. Since in this work we have always thought in terms of current, also in this part we assume the current as input parameter. In the inductor's optimization a current of 1230 [A] was given. Supposing we can provide a maximum current of 1500 [A] – limit given by the maximum power available for example – we would like to investigate, reducing the heating time, how the energy consumption varies with the heating accuracy. The heating process is simply characterized by one interval with given current and one soaking interval.

In summary, the intervals in which vary the two design variables are summarized in Table 9.

Here, the goal functions are:

$$f_A = f_1 + f_2 + f_3$$
$$f_B = \int_{t_{heat}} E\, dt \qquad (10)$$

Where f_1, f_2, f_3 are the objectives shown in (8). Since an excessive overheating of the billet would be not acceptable, a maximum admissible temperature of 1300 [°C] was set. If during the heating, any point of the billet overcomes 1300 [°C], the solution is considered not feasible. Figure 11 shows the Pareto fronts' trend in the case of both, NGSA-II and AMALGAM*, with a population of 30 individuals, after 50 generations.

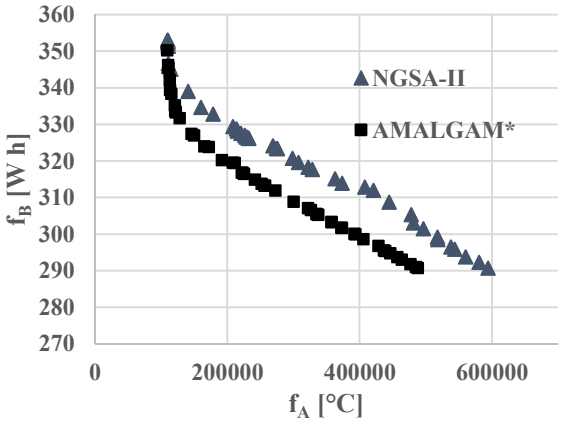

Fig. 11. Objective functions after 50 generations

Tab. 9. Possible intervals for heating and soaking time

t_{ON}	t_{OFF}
30-65 [s]	0.1-15 [A]

Tab. 10. Minimum value of f_A with the two codes.

	t_{ON} [s]	t_{OFF} [s]
NGSA-II	42.0	6.6
AMALGAM*	41.4	5.5
	f_A[°C]	**f_B [Wh]**
NGSA-II	109342	353.0
AMALGAM*	108882	350.2

The estimated Pareto front obtained with AMALGAM* dominates the NGSA-II's one. The best heating accuracy (minimum f_A) reached by the two codes is shown in Table 10. In the "normal" heating mode described in the paragraph 3.4, f_A would value 100671 [°C] and f_B 355.8 [Wh]. If on one side the results of optimal control don't bring any improvement in terms of heating accuracy, on the other hand, with a small worsening of the temperature profile, an important reduction of time and energy consumption could be obtained.

Conclusions

Using a multimethod optimization search has been found to be a more successful solution in both test and real cases compared to the well-known NGSA-II. Even if in this work the performances were compared in the case of same number of field evaluations, the main advantage of AMALGAM* is the reduction of the computation time especially in real case problems.

References

[1] Di Barba P., Dughiero F., Forzan M., Sieni E., *Migration-corrected NGSA-II for improving multi-objective design optimization in electromagnetics,* International Journal of Applied Electromagnetics and Mechanics 51, 2016, pp. 161-172.

[2] Deb K., *A Fast and Elitist Multi-Objective Genetic Algorithm: NGSA II*, IEEE, Transactions one evolutionary computation, April 2002, VOL. 6, N. 2.

[3] Di Barba P., Forzan M., Sieni E., *Multi-objective design of a power inductor: A benchmark problem of inverse induction heating,* COMPEL – The International Journal for Computation and Mathematics in Electrical and Electronic Engineering 33, 2014, pp. 1990-2005.

[4] Reyes-Sierra M., Coello Coello C.A., *Multi-Objective Particle Swarm Optimizers: A Survey of the State-of-Art,* Internation Journal of Computation Intelligence Research, Vol. 2, No. 3 2006, pp. 287-308.

[5] Nanbo J., Yahya R. S., *Particle Swarm Optimization for Antenna Designs in Engineering Electromagnetics*, Journal of Artificial Evolution and Applications, Volume 2008, pp. 2-10.

[6] Di Barba P., Dughiero F., Mognaschi M. E., Savini A., Wiak S., *Biogeography-Inspired Multi-Objective Optimization and MEMS Design*, IEEE Transactions on Magnetics, March 2016, Vol. 52, No. 3.

[7] Wolpert D. H., Macready W. G., *No Free Lunch Theorems for optimization*, IEEE, Transactions one evolutionary computation, VOL. 1, N. 1, April 1997.

[8] Vrugt J. A., Robinson B., *Improved evolutionary optimization from generically adaptive multimethod search,* PNAS, Vol. 104, January 2007.

[9] Dan Simon, *Biogeography-Based Optimization*, IEEE Transactions on Evolutionary Computation, Vol. 12, No. 6, December 2008.

[10] Sieni E., Di Barba P., Forzan M., *Migration NGSA: method to improve a non-elitist searching of Pareto front, with application in magnetics,* Inverse Problem in Science and Engineering, 2016, Vol. 24, No. 4, pp. 543-566.

[11] Li H., Zhang Q., *Multiobjective Optimization Problems with Complicated Pareto Sets, MOEA/D and NSGA-II*, IEEE Transactions on evolutionary computation, Vol. 13, No. 2, April 2009, pp. 284-302.

[12] Baldan M., Steinberg T., Baake E., *Numerical and practical investigation of tailored heating process for forging parts,* Proceedings of XVIII International UIE Congress, Hannover, June 6-9, 2017, pp. 338-345.

[13] Guo Y.F., Hua M., Osman F.H., *A preliminary analysis of thermal differential forging – a ring hearer or locally heated cylindrical rod*, Proceedings of the 24th International Thermal Conductivity Conference and 12th International Thermal Expansion Symposium, Pittsburgh, PA, October 26-29, 1997, pp. 731-745.

[14] Kayatürk K., Kurt A., Weidig U., Steinhoff K., E. Tekkaya A., *Simultaneous cold and hot forging in a single forming step – principle, possibilities and limitations*, Proceedings of 3th International Conference on Industrial Tools, Slovenia, April 22-26, 2001, pp. 97-100.

Authors

MSc. Baldan, Marco — E-mail: baldan@etp.uni-hannover.de
Dipl.-Ing., Steinberg, Thomas — E-mail: steinberg@etp.uni-hannover.de
Prof. Dr.-Ing. Baake, Egbert — E-mail: baake@etp.uni-hannover.de
Institute of Electrotechnology
Leibniz University of Hannover
Wilhelm-Busch-Str. 4
D-30167 Hannover, Germany